

Fragmentation and cluster formation in the Infrared Dark Cloud G14.225–0.506

Author: Eduard Torres i Duran.

*Facultat de Física, Universitat de Barcelona, Diagonal 645, 08028 Barcelona, Spain.**

Advisor: Gemma Busquet Rico

Abstract: We obtained images of the G14.2 Hub-S with data acquired by ALMA. The visibilities were weighted naturally and with `robust=0` with the task `tclean` of CASA to get different spatial resolutions (160 and 64 AU, respectively). We identified 22 sources with the tool PyBDSF and we estimated their masses and sizes. We found that most of the sources correspond to low-mass protostellar disks but there is a large mass reservoir in the envelope that can feed the protostar to become high-mass stars.

I. INTRODUCTION

Even though stars represent the 99% of the mass in the Galaxy, they do not even reach the 1% of its volume. The Interstellar Medium (ISM) consists of gas that fills most of the space. Stars form within molecular clouds, the densest and coolest regions of the ISM. They have masses $\sim 10^3 - 10^7 M_\odot$ and span several parsecs. Molecular clouds fragment hierarchically into smaller structures called dense cores, that eventually collapse forming a protostar or a binary/multiple system. It explains why stars do not form solitary but in clusters.

The protostar can emit by the heating coming from its contraction, not by thermonuclear reactions (as mature stars do). It collects the surrounding material of the envelope, which falls into the equatorial plane of the rotating core forming an accretion disk. Further accretion proceeds from the disk towards the protostar. When all the mass from the envelope and the disk has been accreted by the core, it can still contract until it becomes a star.

The Infrared Dark Cloud (IRDC) G14.225–0.506 (hereafter G14.2) is the southwest extension of a large molecular cloud associated with the Omega Nebula at the M17 region, at a distance of 1.6 kpc from us [9]. The region consists of two hub-filament systems [3, 4], being hubs the main sites of star formation. Observations with the Submillimeter Array (SMA) at 1.3 mm (angular resolution $\sim 1.5''$) and the Atacama Large Millimeter/submillimeter Array (ALMA) at 3 mm (angular resolution $\sim 3''$) reveal that both hubs fragment into multiple dense cores [2, 6].

In this work we focus on the southern hub, called Hub-S, which contains an embedded cluster with masses ranging from $0.7 M_\odot$ up to $\sim 18 M_\odot$ [2]. Previous works suggests that massive O-type stars have not been produced yet in this region [8], but they can still form by accreting a significant amount of gas from the surrounding material [6]. Here we present high angular resolution observations carried out with ALMA towards G14.2 Hub-S in

order to investigate the mass reservoir at different spatial scales and assess whether the embedded cores may become massive enough to form high-mass stars (i.e., stars with masses $> 8 M_\odot$).

II. OBSERVATIONS

G14.2 Hub S was observed with ALMA [11] at 226.15 GHz using two configurations (C5 and C8) as part of the project “The formation of high-mass binary systems by core/disk fragmentation” (project code: 2017.1.00237.S, PI: Patricio Sanhueza). ALMA works with different spatial configurations of the antennas, which can be moved from 150 m up to 16 km. The longer the maximum distance between antennas, the higher the resolution of our images.

In order to obtain the images from the collected visibilities, we used the task `tclean` of the *Common Astronomy Software Applications* (CASA [12]). First, `tclean` reconstructs a dirty image from the visibilities map by applying the Fourier transform. We used both configurations (C5+C8) to create a combined image. There are several options to assign different weights (different responses of the measurement system) across the input point distribution during the process. The uniform weighting multiplies each visibility by the same value so we get higher resolution (smaller beam) but less sensitivity. The natural weighting takes into account the data density of the visibilities, so it gives high sensitivity images to the detriment of a larger beam (appropriate to detect the envelope of the sources). The Briggs weighting allows intermediate weightings between natural and uniform by setting a robust coefficient $R \in [-2, +2]$, being -2 the uniform and $+2$ the natural weighting.

Then, `tclean` reduces the noise of the images by applying Högbom’s CLEAN algorithm[5]. In each iteration, this algorithm finds the highest value of the dirty image in order to find the sources, subtracts a small fraction of its brightness and replaces it to the clean image. It stops when there is no peak last below a threshold specified by us, which has to be around twice or thrice the background noise.

We made two images with different weighting (natural and `robust=0`, see Table I) in order to obtain distinct

*Electronic address: etorredu16@alumnes.ub.edu

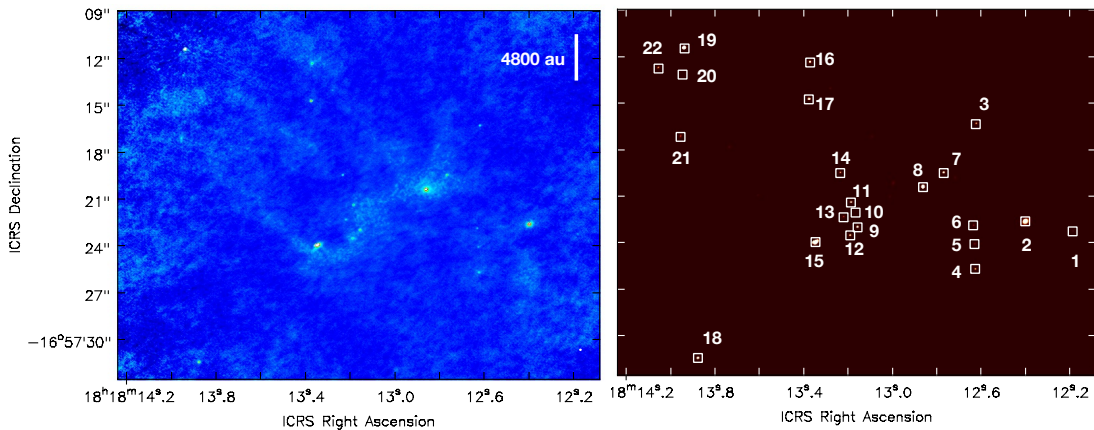


FIG. 1: *Left*: ALMA 1.3 mm dust continuum image of G14.2 Hub-S obtained with natural weighting. The synthesized beam is shown in the bottom right corner of the image. *Right*: Identified sources by PyBDSF (see Table II), highlighting their location with white squares.

resolutions to study the emission from the envelope and the emission from the accretion disks.

TABLE I: ALMA imaging parameters from C5+C8 configurations

Image weighting	Beam (″×″)	P.A. (°)	rms (μJy/beam)
natural	0.105×0.088	-83.01	50
robust=0	0.040×0.037	89.85	70

III. RESULTS

Figure 1 (left panel) shows the 1.3 mm image toward G14.2 Hub-S obtained with natural weighting. Most of the sources are grouped and in some cases they appear aligned in rows of 2, 3 and up to 5 cores. In Fig. 2 we present zoom-in images of the central part of Hub-S, showing both the natural weighted image (color scale and white contours) and the robust=0 image (black contours).

A. Source Identification

In order to identify the sources we used the *Python Blob Detector and Source Finder* tool (PyBDSF [13]). First, PyBDSF reads the image created by CASA and it computes the root mean square (rms) –a quantity that gives an idea of the average background noise– with a squared 2D box that scans across the map. We can define the box size (usually the size of the artifacts, we set 20 pixels) and the number of pixels the box has to jump in consecutive measures (a third or a fourth of the box size). Proper values of these inputs are crucial to compute correctly the rms, so we opted to use an adaptive box that is reduced in size near bright sources. Once we have the rms, PyBDSF splits the pixels higher than a threshold value (in our case 3.5σ , where σ is the rms

of the map) from the background noise and they constitute emission islands. Then, the islands are fitted with multiple Gaussians, which are grouped into sources.

We applied PyBDSF to the natural image first due to its higher sensitivity and we got a new map of 22 identified sources (see Fig. 1-right panel) and a list of their properties: peak position (R.A. and Dec.), total flux, peak flux, deconvolved angular size (major and minor axis), and position angle (P.A.). Once the sources were identified, we obtained their parameters in robust=0 image by fitting a 2D Gaussian function with CASA. Table II lists the main properties of the 22 sources.

B. Mass estimation

We estimated the mass M of each source using the expression below

$$M = \frac{c^2}{2k_B\nu^2} \frac{S_\nu d^2}{\kappa_\nu T_d}, \quad (1)$$

where $c^2 = 8.99 \times 10^{20} \text{ cm}^2 \text{ s}^{-2}$ is the squared speed of light in vacuum, $k_B = 1.38 \times 10^{-16} \text{ cm}^2 \text{ g s}^{-2} \text{ K}^{-1}$ is the Boltzmann constant, $\nu = 2.2615 \times 10^{11} \text{ s}^{-1}$ is the frequency of our observations, S_ν is the flux listed in Table II, d is the distance to the source ($1.6 \text{ kpc} = 4.937 \times 10^{21} \text{ cm}$), κ_ν is the dust mass opacity coefficient, and T_d is the dust temperature. We adopted a dust mass opacity coefficient $\kappa_{1.3 \text{ mm}} = 0.899 \text{ cm}^2 \text{ g}^{-1}$ [7] that corresponds to coagulated grains with thin ice mantles in cores of densities $\sim 10^6 \text{ cm}^{-3}$. We assumed a constant dust temperature of 25 K for all cores [see e.g., 6]. Finally, we obtain the following expression:

$$M(M_\odot) = 3.262 \times 10^{-2} S_\nu (\text{mJy}) \quad (2)$$

Table II lists the estimated masses from the natural weighted and robust=0 images. We obtained masses from $0.01 M_\odot$ up to $1.3 M_\odot$. Masses in the robust=0 map

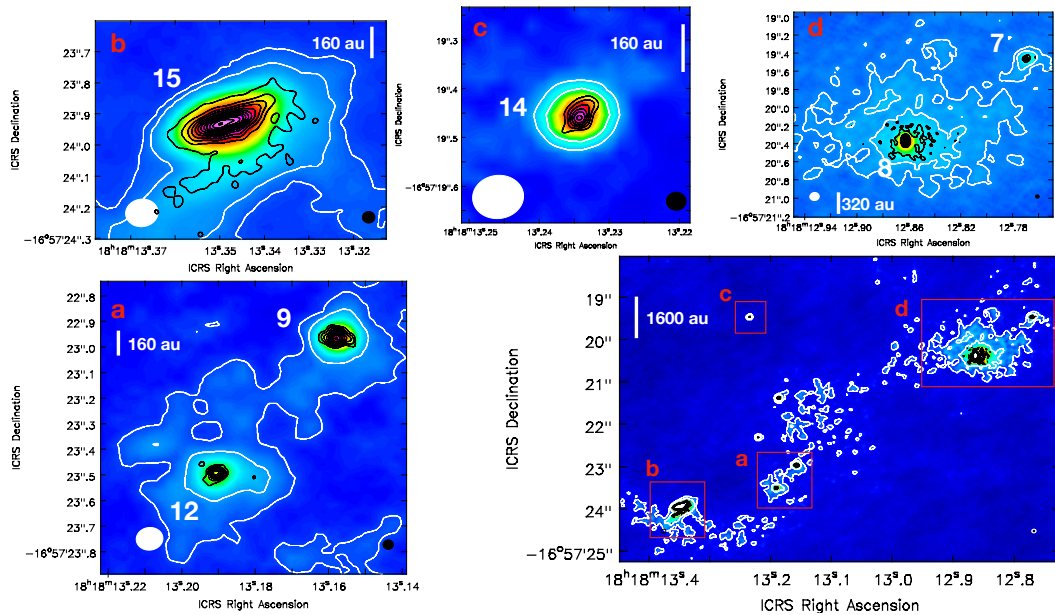


FIG. 2: Close-up image of the central part of Hub S (bottom right panel). Boxes indicate zoom-in images (a, b, c, and d) with the Source ID indicated. In all panels white contours are 3 and 6 σ level of the natural weighted image, where σ is the rms of map (see Table I) and black contours is the robust=0 image. The linear scale is indicated in each panel. The ALMA synthesized beam are shown in the bottom left (natural) and bottom right (robust=0) corners of each image.

tend to lower than natural weighted masses, as expected. The robust=0 image filters out the extended emission of the envelope and the main contribution to the mass is from the disk. In a few cases the robust=0 mass is comparable (or even greater) than the natural mass (Source ID 3, 9, 14, 19) because the source is unresolved (see e.g., Fig. 2-panel c for Source ID 14). Figure 3 (top) shows the histogram of the mass distribution for the detected sources. Overall, the number of sources decreases as mass increases, with the exception of the most massive objects. However, this increase is due to a different binning in the mass distribution, hence it is not “real”. Due to the uncertainty in the dust mass opacity coefficient and the temperature, the values of the derived masses are good to within a factor of 2.

We compared our results to two other works at different spatial scales (2400 AU [2] and 640 AU [1]). As can be seen in Fig. 4, the masses estimated with the SMA data are one order of magnitude greater than the ones estimated with ALMA at scales < 1000 AU. This indicates that there is a large mass reservoir around the compact sources identified by us. This material can still be added eventually to the disk and to the protostar itself. In fact, the fraction of mass that is in the disk with respect to the envelope mass (see Table II) is around 10% or even less. Therefore, all these protostars can still grow in mass and become massive stars.

C. Size estimation

PyBDSF gives an estimation for the deconvolved major and minor axis $DC_{maj,min}$, in units of arc-seconds, of the

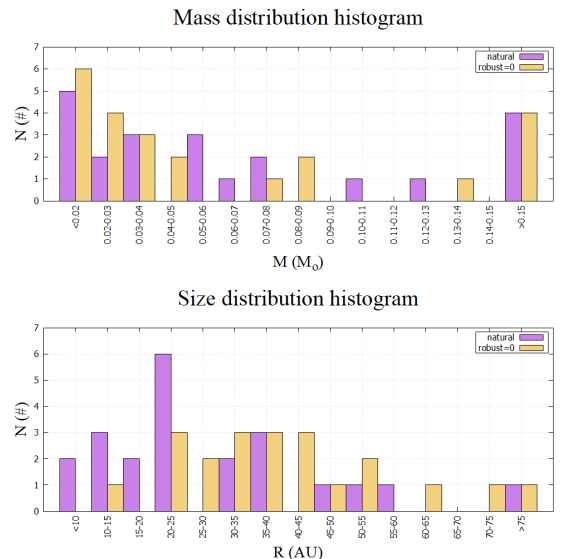


FIG. 3: Histograms for the mass (top) and radius (bottom) distribution for the natural image (purple) and robust=0 image (orange).

source ellipses. We converted these angular quantities into spatial longitudes $R_{maj,min}$, the major and minor radius, as follows:

$$R_{maj,min}(\text{AU}) = \frac{1}{2}DC_{maj,min}(\text{arcsec})d(\text{pc}), \quad (3)$$

where $d = 1600$ pc is the distance to G14.2 [9]. Then, we computed the source radius R reported in Table II

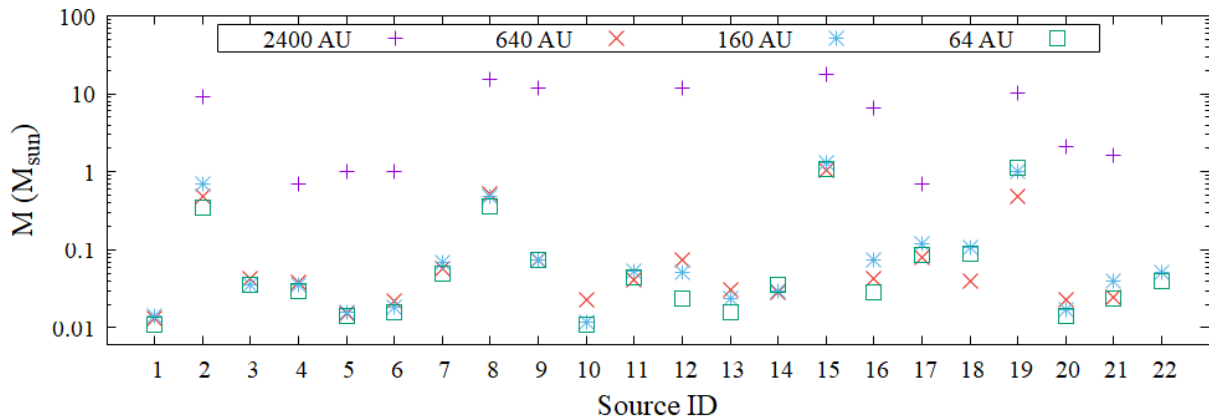


FIG. 4: Mass distribution for the natural image (160 AU) and robust=0 image (64 AU), compared with previous works: TFG of A. Brichs (640 AU, [1]) and SMA observations (2400 AU, [2]).

as the geometrical mean of the major and minor radius,

$$R = \sqrt{\frac{1}{2}R_{maj}R_{min}}.$$

As can be seen in Table II and Fig 3 (bottom), we obtained sizes from 10 AU to 80 AU (size range is narrower in robust=0 data). The median radius is 39 ± 13 AU (natural image) and 26 ± 9 AU (robust=0 image). The major tendency for our results is that source sizes in the natural weighted map are higher than their corresponding robust=0 size, in agreement with the mass behaviour.

D. Multiplicity

Comparing our ALMA results to the SMA observations at lower resolution (Fig. 5), we can assess how many ALMA sources constitute the SMA cores [2]. We identify 7 single protostars (S), 2 binary systems (B), 2 triple systems (T), none quadruple (Q) and 1 quintuple. The multiplicity fraction (MF) is the ratio of multiple systems over all of them (including the single ones) and can be thought of as the probability of a given system having companions. It is defined as:

$$MF = \frac{B + T + Q + \dots}{S + B + T + Q + \dots} = 0.42 \pm 0.14 \quad (4)$$

The companion star fraction (CSF) is the average number of companions per system:

$$CSF = \frac{B + 2T + 3Q + \dots}{S + B + T + Q + \dots} = 0.83 \pm 0.11 \quad (5)$$

The uncertainties are computed using the Wilson score interval [10].

IV. CONCLUSIONS

We studied the IRDC G14.2 Hub-S at different spatial scales to estimate the mass, size and multiplicity of the cores and their surrounding material. From our work, we found mostly low-mass objects except for a couple of cores with masses $\sim 1 M_{\odot}$ (Source ID 15, 19). Concerning

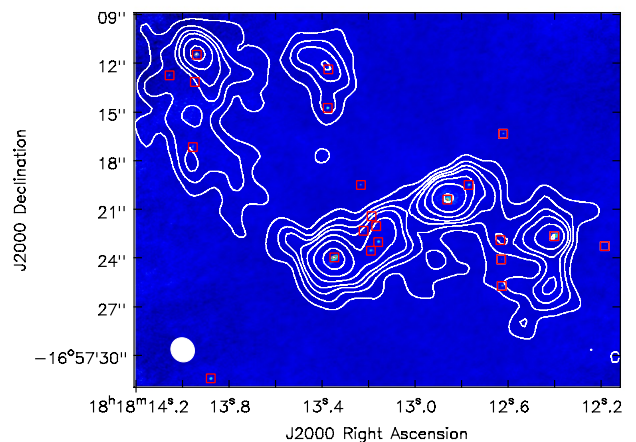


FIG. 5: ALMA 1.3 mm image overlaid with the SMA 1.3 mm image (contours) at $1.5''$ resolution [2]. Contours are 3, 6, 9, 12, 18, 28 and 48 times the rms of map ($\sim 1 \text{ mJy beam}^{-1}$). The ALMA and SMA synthesized beams are shown in the bottom right and bottom left corners, respectively. The 22 identified sources are indicated with red squares.

to the size, we obtained disk radii ranging from 10 AU to 80 AU. In regard to multiplicity, we could observe at high angular resolution that several cores observed with SMA are in fact multiple systems (e.g., Source ID 9, 12) and some were still single sources (e.g., Source ID 15).

Even if our cluster is constituted by low-mass disks, one can say from $\frac{M_{\text{disk}}}{M_{\text{env}}}$ values, that they have still a large amount of material in the envelope. We do not know yet how much of this envelope will dissipate or be accreted to the disk but G14.2 Hub-S might end up forming a cluster of high-mass stars.

TABLE II: ALMA 1.3 mm continuum sources toward G14.225-0.506

Source ID	R.A.(ICRS)	Dec. (ICRS)	Flux		Mass		R		P.A.	$\frac{M_{\text{disk}}}{M_{\text{env}}}$
	(18 ^h 18 ^m)	(-16 [°] 57 ['])	natural	robust=0	natural	robust=0	natural	robust=0	([°])	(%)
	(s)	(^{''})	(mJy)	(mJy)	(M_{\odot})	(M_{\odot})	(AU)	(AU)		
1	12.185	23.220	0.42 ± 0.01	0.34 ± 0.06	0.014	0.011	- ^a	24 ± 8	0 ± 30	...
2	12.401	22.593	21.7 ± 1.2	10.8 ± 0.7	0.708	0.353	80 ± 6	58 ± 7	115 ± 4	3.8
3	12.622	16.298	1.06 ± 0.09	1.08 ± 0.12	0.035	0.035	28 ± 5	20 ± 6	128 ± 13	...
4	12.626	25.669	1.11 ± 0.12	0.91 ± 0.13	0.036	0.030	32 ± 6	23 ± 6	60 ± 20	6.0 ^b
5	12.629	24.047	0.5 ± 0.1	0.43 ± 0.07	0.016	0.014	32 ± 10	9 ± 5	140 ± 30	6.0 ^b
6	12.634	22.853	0.54 ± 0.03	0.48 ± 0.05	0.018	0.016	14 ± 10	8 ± 6	0 ± 20	6.0 ^b
7	12.769	19.457	2.09 ± 0.12	1.49 ± 0.09	0.068	0.049	35 ± 4	13 ± 4	115 ± 7	7.3 ^b
8	12.862	20.370	15.0 ± 0.6	11.1 ± 0.3	0.489	0.361	48 ± 5	31 ± 3	170 ± 20	13.1 ^b
9	13.157	22.962	2.24 ± 0.15	2.28 ± 0.18	0.073	0.074	36 ± 5	35 ± 5	88 ± 10	13.1 ^b
10	13.166	22.018	0.38 ± 0.07	0.33 ± 0.06	0.012	0.011	20 ± 30	34 ± 8	120 ± 70	13.1 ^b
11	13.186	21.367	1.63 ± 0.09	1.34 ± 0.07	0.053	0.044	28 ± 3	12 ± 3	106 ± 9	13.1 ^b
12	13.190	23.496	1.56 ± 0.18	0.73 ± 0.08	0.051	0.024	44 ± 7	17 ± 5	101 ± 13	13.1 ^b
13	13.220	22.302	0.74 ± 0.06	0.5 ± 0.09	0.024	0.016	36 ± 5	20 ± 9	99 ± 9	13.1 ^b
14	13.234	19.455	0.93 ± 0.03	1.06 ± 0.11	0.03	0.035	24 ± 4	22 ± 5	119 ± 10	...
15	13.348	23.927	39.6 ± 0.9	33.3 ± 0.8	1.292	1.086	60 ± 4	52 ± 4	108 ± 1	6.1
16	13.372	12.342	2.3 ± 0.3	0.87 ± 0.12	0.075	0.028	53 ± 9	14 ± 6	180 ± 140	4.1 ^b
17	13.376	14.727	3.69 ± 0.14	2.67 ± 0.19	0.120	0.087	20 ± 2	19 ± 3	175 ± 8	4.1 ^b
18	13.877	31.392	3.3 ± 0.2	2.8 ± 0.4	0.108	0.09	41 ± 5	35 ± 8	116 ± 10	...
19	13.939	11.427	31.2 ± 0.4	33.8 ± 0.9	1.018	1.104	30 ± 2	35 ± 3	118 ± 2	11.2 ^b
20	13.946	13.092	0.51 ± 0.14	0.44 ± 0.16	0.017	0.014	70 ± 30	- ^a	154 ± 13	11.2 ^b
21	13.955	17.120	1.2 ± 0.3	0.7 ± 0.4	0.039	0.024	50 ± 20	46 ± 4	160 ± 20	1.5
22	14.055	12.704	1.6 ± 0.3	1.2 ± 0.5	0.052	0.04	40 ± 20	21 ± 15	130 ± 20	11.2 ^b

Notes. ^a Source cannot be resolved. ^b We assumed a common envelope mass [2] and the sum of M_{disk} of the companions.

Acknowledgments

This project would not be possible without the immeasurable help of Dra. Gemma Busquet. I appreciate her

guidance and support during the semester, specially at its final stages.

-
- [1] Brichs, A. “Identification of the stellar population in the massive cloud IRDC G14.225”. 2021, Bachelor Thesis (UAB).
- [2] Busquet, G., Estalella, R., Palau, A. et al. “What Is Controlling the Fragmentation in the Infrared Dark Cloud G14.225-0.506?: Different Levels of Fragmentation in Twin Hubs”. *The Astrophysical Journal*. **819**, 139 (2016)
- [3] Busquet, G., Zhang, Q., Palau, A. et al. “Unveiling a Network of Parallel Filaments in the Infrared Dark Cloud G14.225-0.506”. *The Astrophysical Journal Letters*. **764**, L26 (2013).
- [4] Chen, H.-R. V., Zhang, Q., Wright, M. C. H., Busquet, G. et al. “Filamentary Accretion Flows in the Infrared Dark Cloud G14.225-0.506 Revealed by ALMA”. *The Astrophysical Journal*. **875**, 24 (2019).
- [5] Högbom, J. (1974), “Aperture synthesis with a non-regular distribution of interferometer baselines”, *Astrophys. J. Suppl. Ser.*, 15, 417-426.
- [6] Ohashi, S., Sanhueza, P., Chen, H.-R. V. et al. “Dense Core Properties in the Infrared Dark Cloud G14.225-0.506 Revealed by ALMA”. *The Astrophysical Journal*. **833**, 209 (2016)
- [7] Ossenkopf, V. & Henning, Th. “Dust opacities for protostellar cores”. *Astronomy & Astrophysics*. **291**, 943-959 (1994).
- [8] Povich, M. S., Townsley, L. K., Robitaille, T. P. et al. “Rapid Circumstellar Disk Evolution and an Accelerating Star Formation Rate in the Infrared Dark Cloud M17 SWex”. *The Astrophysical Journal*. **825**, 125 (2016)
- [9] Zucker, C., Speagle, J. S., Schlafly, E. F. et al. “A compendium of distances to molecular clouds in the Star Formation Handbook”. *Astronomy & Astrophysics*. **633**, A51 (2020).
- [10] Wilson, E. B. 1927, “Journal of the American Statistical Association”, 22, 209
- [11] www.almaobservatory.org
- [12] <https://casa.nrao.edu>
- [13] <https://www.astron.nl/citt/pybdsf/>